Topology Optimization and Additive Manufacturing for Electrohydraulic Actuators in Hydraulic Foot Robots

Chikun Gong, Longkun Li, Lipeng Yuan, and Yuhang Yang

***Abstract*—In recent years, hydraulic quadrupedal robots have received increasing attention for their good adaptability and high load carrying capacity. However, weight management remains a key challenge for mobile robotic systems, especially considering the limited on-board energy. Topology optimization has now become a tool to significantly reduce weight and size while maintaining structural integrity. A comprehensive design methodology for electro-hydraulic actuator structures for quadruped robots that integrates topology optimization design, internal runner optimization and additive manufacturing is proposed. The use of topology optimization not only ensures the mechanical properties required for the practical application of the electrohydraulic actuator, but also reduces the mass and volume of the electrohydraulic actuator by more than 15.2%. Through the optimized design of the bionic flow channel, the pressure loss of the rotor is reduced by 40%, and the energy transfer efficiency is significantly improved. In addition, this work successfully demonstrates the integration of topology optimization and additive manufacturing, which provides new ideas for the study of advanced electrohydraulic actuators for legged robots. This innovation not only improves the performance of hydraulic quadruped robots, but also establishes a new paradigm for the design and fabrication of complex robotic systems.**

***Index Terms*—Hydraulic foot robots, Electro Hydraulic Actuators, Bionic vascular flow channel, Topology optimization, Additive manufacturing**

I. Introduction

IN recent years, the Italian Institute of Technology (IIT), in collaboration with Moog, has integrated intelligent actuators (ISAs) into the HyQ-real robot [1]. This advancement significantly improved the power-to-weight ratio of the system, resulting in a highly reliable and efficient hydraulically driven mobile system. However, limited energy access remains a key challenge for robots, especially for those operating at high speeds or under heavy load conditions.

Weight reduction is widely recognized as a key method to minimize additional on-board energy consumption.Elasswad et al. used neural algorithms to analyze and improve the original mechanical structure of the humanoid robot HYDROïD, thus optimizing its actuators [2]. In order to reduce the weight, they replaced some metal parts with carbon fiber and succeeded in reducing the weight of the robot from 125 kg to 97 kg [3-4]. Similarly, Hyon et al. (2013) also optimized the actuator of the hydraulic leg by replacing the linkage mechanism in the actuator with a carbon fiber reinforced plastic material to achieve a weight reduction effect between the actuator and the rest of the equipment and showed the results of the single-leg experiments [5]. MiniHyQ is the lightest hydraulic quadrupedal robot currently available, with a total weight of only 35 kg. It uses minimal hydraulic pumps and other hydraulic components to fulfill its work requirements [6]. It uses a more compact mechanical structure to minimize unnecessary materials. In the hydraulic system, a centralized valve block replaces the distributed valve block, resulting in a smaller size and weight of the block with the same functionality, further reducing the weight of the quadruped robot. Semini et al. (2015) optimized the manifold of the HyQ2Max robot by improving the conventional manifold with the design concept of 3D printing. The conventional manifold has low material utilization and auxiliary holes [7]. However, all the above methods of lightweighting hydraulic systems use trial and error, and then test the appropriate working conditions to determine if the part meets the operating requirements [8]. Although all the above studies have achieved satisfactory results in terms of weight reduction, most of them are still based on experience and are not user-friendly for engineers.

Currently, with the gradual maturity of additive manufacturing technology and topology optimization design methods, the integration of topology optimization and additive manufacturing has been widely promoted and applied in aerospace and automotive engineering [9].

For example, the Houston Research Laboratory in the United States, in collaboration with Morf 3D, a 3D printing design software company and aerospace manufacturing service provider, developed an aircraft fuel heat exchanger with a spiral internal structure. This innovation resulted in a 146% increase in surface area, a 50% reduction in wall thickness, and a 300% increase in heat transfer rate [10]. Similarly, RUAGSpace in Europe used selective laser

Manuscript received December 24, 2024; revised May 4, 2025.

This work was supported by the National Key Re-search and Development Program (No. 2022YFB4703400) and Jiangsu Province general program of China (No. BK20211028).

Chikun Gong is an associate professor at the College of Mechanical Engineering, University of Shanghai for Science and Technology, Shanghai 200093, China (e-mail: gongchikun@126.com).

Longkun Li is a postgraduate from the College of Mechanical Engineering, University of Shanghai for Science and Technology, Shanghai 200093, China (e-mail: 1514857965@qq.com).

Lipeng Yuan is an associate professor at the College of Mechanical and Electrical Engineering, Harbin Institute of Technology, Harbin, 150001, China (corresponding author to provide phone: 86-13611644083; e-mail: hitylp@126.com).

Yuhang Yang is a postgraduate from the College of Mechanical Engineering, University of Shanghai for Science and Technology, Shanghai 200093, China (e-mail: 670654265@qq.com).

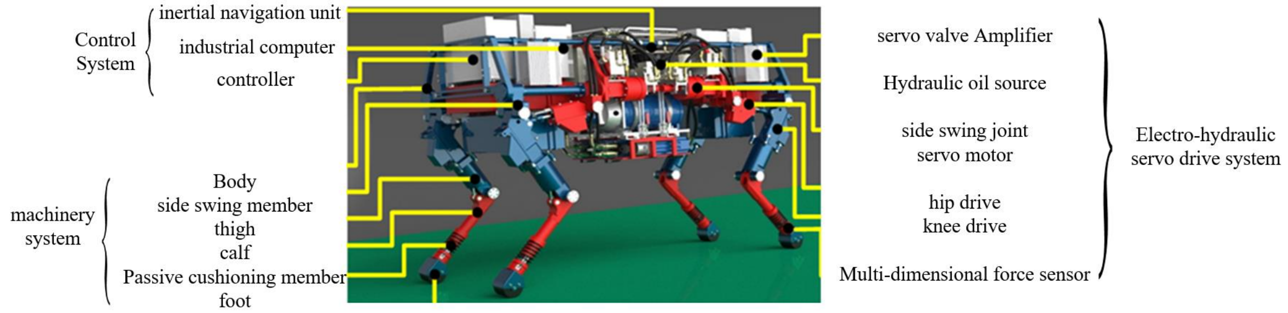

Figure 1 Quadruped robot structure

melting (SLM) technology to fabricate an aluminum alloy antenna mount for an Earth observation satellite [11]. Zhong et al. used additive manufacturing techniques to introduce hybrid mesh structures into lightweight design and combined additive manufacturing with topology optimization techniques to reduce redundant materials in structural components [12]. In the field of topology design, Sanford Meek et al. designed Kagome, cone and hexagonal rhombic unit structures. These structures were used to fabricate (AlSi10Mg) porous grid heat exchangers through SLM equipment to provide technical support for their application in aero-engines [13]. Topology optimization has emerged as a powerful technique for achieving structural lightweighting while maintaining the required level of performance [14], leading to its widespread adoption in various engineering fields [15, 16].

Recently the application of topology optimization and additive manufacturing has been extended to hydraulic quadruped robots with significant progress by Huang et al [17]. Their innovative approach combined additive manufacturing with topology optimization to redesign a hydraulic cylinder end cap, achieving a 50.7% volume reduction by simultaneously optimizing the structural geometry and fluid path. In addition, Hansen and Andersen used topology optimization techniques to optimize the entire hydraulic system, considering individual components and operating conditions. This approach enables the use of the most cost-effective components to meet weight reduction requirements [18]. Kubo et al. applied topology optimization to optimize the internal passages of the manifold to achieve minimum pressure loss [19]. However, the challenge of combining low pressure loss with compact size and reduced mass remains an area for further research.

As described in reference [20], this research focuses on lightweighting techniques for legged robot electro-hydraulic actuators. The research will investigate topology optimization and additive manufacturing techniques for key components of legged robots, with a focus on integrating these two approaches. The main objective is to develop electro-hydraulic actuators characterized by enhanced strength, stiffness and weight reduction, thus addressing the specific technological requirements of legged robotic systems. In addition, this research aims to establish a theoretical foundation and practical framework for lightweight structural design and additive manufacturing of electro-hydraulic actuators, potentially contributing to future technological developments in this specialized field.

II. Mechanical Structure and Actuator Design

A. Robot structure

Fig. 1 illustrates the mechanics of the quadrupedal robot under study, which is characterized by symmetrical design, compactness and dexterity of movement. The robot employs a biologically inspired front-elbow-back-knee structure that mimics the mammalian quadrupedal form. This biomimetic design greatly enhances the system's terrain adaptation, obstacle negotiation, and dynamic stability during locomotion. The integrated robotic platform consists of three core subsystems: a control system, a mechanical system and an electro-hydraulic servo system.

B. The Overall Design of The Electro-Hydraulic Actuator

In quadrupedal robotics research, lightweight and efficient electro-hydraulic actuators are essential for improving the performance of quadrupedal robots. Minimizing the unnecessary material usage, operating power requirement, and device loading capacity of the actuator is one of the main methods to improve the high-power density of the actuator. For the actuator rigid body part, the authors conducted a related lightweighting study, and in the initial phase of the study, the research team developed and designed comprehensive 3D models for each component of the electrohydraulic actuator. Based on the actual manufacturing and material properties, aluminum alloy was selected as the main material for the actuator. Aluminum alloy components offer better weight advantage for the same volume. However, aluminum alloys are not as weldable as steel, making the components unsuitable for welding after forming. The weight of the actuator is further reduced by the replacement of a dense steel material with an ultimate strength of 455 MPa by an aluminum alloy. Although the weight of the actuator has been greatly reduced, there is still much to be optimized, and topology optimization can be effective in achieving this goal. The structure of the machined integrated electrohydraulic actuator is shown in Fig. 2.

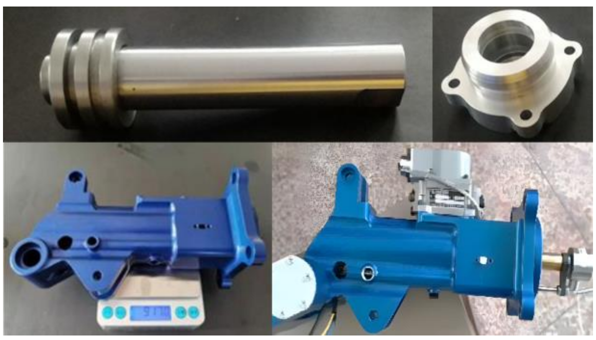

Figure 2 Machining integrated bionic electro-hydraulic actuator

III. Electro-hydraulic Actuator Topology Optimization and Flow Path Optimization Design

A. *Topology Optimization Design*

Prior to topology optimization, a static analysis of the existing integrated electro-hydraulic actuator must be performed. This analysis is an important foundation for the subsequent optimization process, ensuring that structural integrity and performance requirements are met prior to material redistribution.

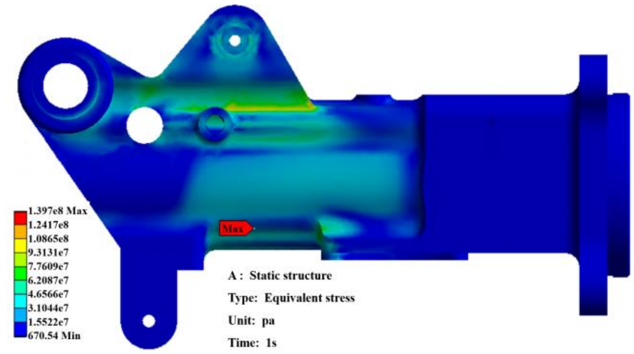

(a) Stress nephogram under working condition 1

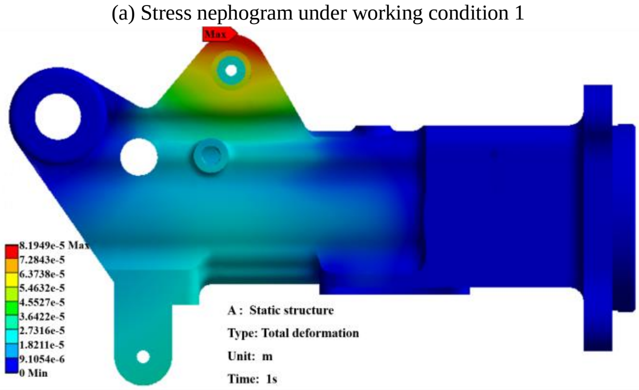

(b) Strain nephogram under working condition 1

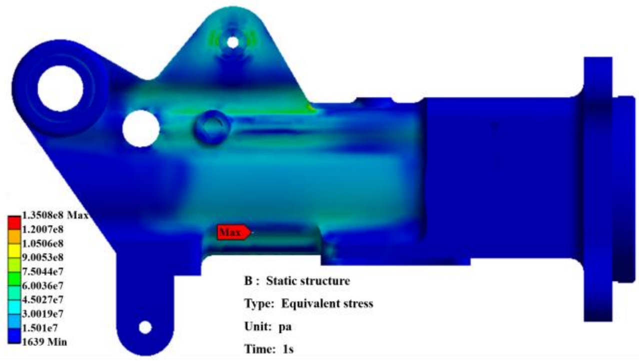

(c) Stress nephogram under working condition 2

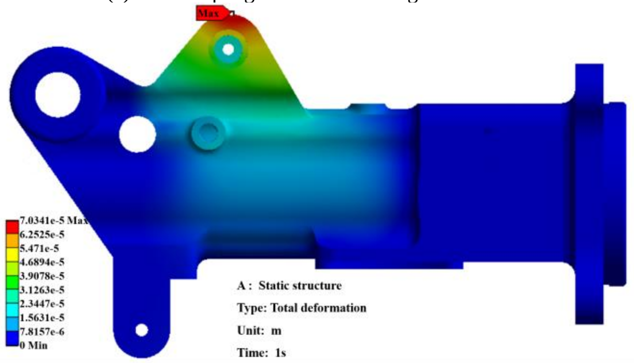

(d) Strain nephogram under working condition 2

Figure 3 Stress-strain diagrams of cylinders under two operating conditions

Since the hydraulic cylinder block is the most complex component in the whole integrated electro-hydraulic actuator and has the largest proportion of its mass, the topology optimization and redesign mainly focus on the cylinder component.

Fig. 3 shows the stress-strain cloud diagrams of the cylinder under two operating conditions. In operating condition 1, the cylinder is subjected to a thrust force of 11,000 N. The stress and strain distributions of the cylinder are shown in Fig. 3(a) and Fig. 3(b), respectively. In working condition 2, the cylinder is subjected to a pulling force of 700 N. The corresponding stress and strain distributions are shown in Fig. 3(c) and Fig. 3(d). In Case 1, the maximum stress of 140 MPa occurs at the intersection of the two internal runners. Similarly, in case 2, the maximum stress occurs at the intersection of the two internal runners with a value of 135 MPa. Since the selected cylinder material has a yield strength of 455 MPa, the current hydraulic cylinder design meets the required safety and performance criteria.

Based on the results of the static analysis, it can be inferred that the material on both sides of the cylinder is most likely to be removed during the structural optimization process. This is since these areas have negligible stress concentrations and are therefore ideal areas for material reduction without compromising structural integrity.

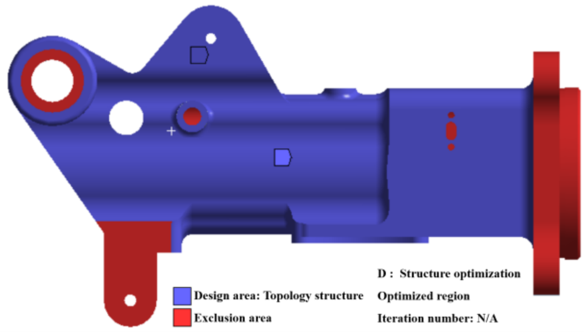

Figure 4 Cylinder bore optimization area setting

The optimized areas of the cylinder were carefully selected as shown in Fig. 4. The oil transfer passages were designated as no-go areas for optimization; these passages were designed integrally within the cylinder while remaining consistent with the external structure of the cylinder. The rest was set as the design domain. Fig. 5 shows the evolution of the interpolated density contour plots corresponding to the optimization results of the different iteration steps.

By analyzing the final topology optimization results, there are limited areas available for optimization. The main area of material reduction is located on the left side in contact with the rotating oil distribution shaft. In addition, a small portion of the material was also removed from the cylinder skin surface. However, the overall optimization effect was not significant. The main reason for this result was the presence of internal runners and the process holes required to create them. These features limited the extent to which material could be removed without compromising functionality. To address this limitation, it was necessary to redesign the runner using an additive manufacturing approach. This approach allows for more complex internal geometries, improved optimization results, and further weight reduction of the cylinder structure.

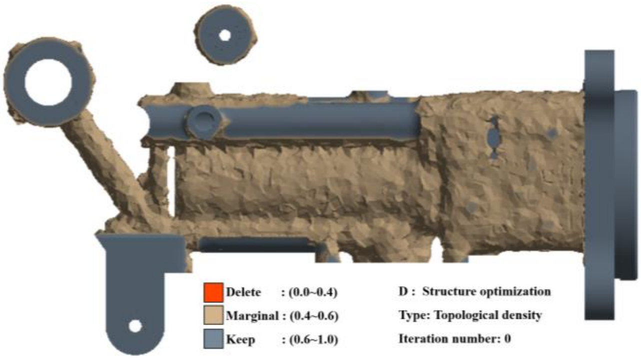

(a)Step1

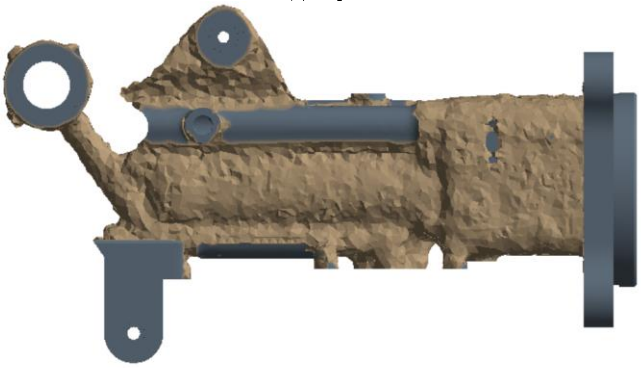

(b) Step2

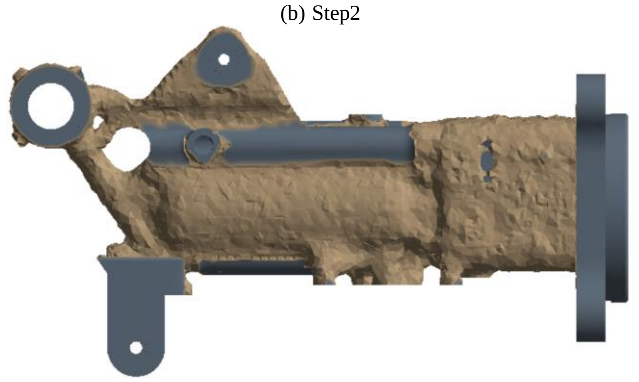

(c) Step3

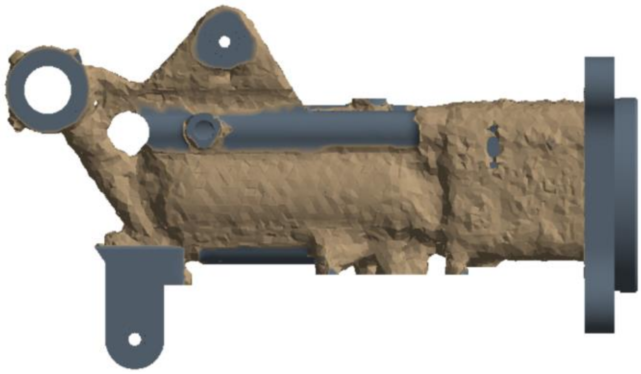

(d) Step4

Figure 5 Optimized density cloud images under different iterative steps

B. *Runner Optimization Design*

Original Runner Design

Conventional electro-hydraulic actuators typically utilize hydraulic hoses connected to a hydraulic fluid source to supply oil to the actuator. To solve the “heavy” and “messy” problems associated with hydraulic flow paths, machined actuators utilize a rotary oil distribution structure. As shown in Fig. 6, the oil distribution shaft is attached to the end of the cylinder of the actuator. This design eliminates the need for pipe fittings and other structures on the actuator, which reduces the risk of leakage and enables a tubeless design of the actuator.

Fig. 7 shows the internal structure and runner distribution of the designed integrated electrohydraulic actuator. The connection between the inlet and outlet positions was realized by machining processes such as drilling and boring. However, the runner distribution was not optimally adjusted. Although the oil ring cavities were effectively utilized, the large corners of the machined runners would negatively affect the oil transfer efficiency. Therefore, it is necessary to optimize the design of the runner.

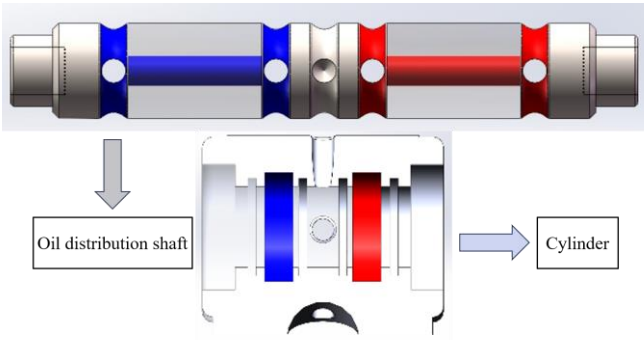

Figure 6 Rotary oil distribution structure of electro-hydraulic actuator

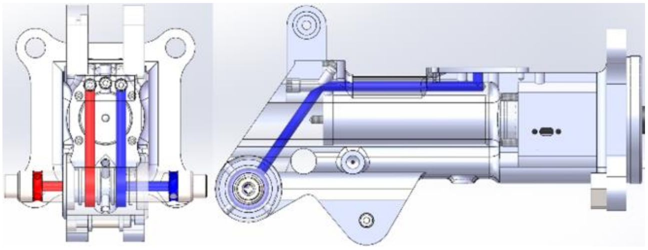

Figure 7 Runner distribution in integrated electro-hydraulic actuator

Runner Optimization Design

The idea of runner optimization mainly starts from the cross-sectional area. Considering that the hydraulic runners overlap with the cylinder wall, not only can the weight be reduced, but also the runners can be attached to the outside of the cylinder wall to form a reinforcement, so as to achieve the purpose of increasing strength. In addition, the principle of bionics can be used to optimize the runner design with reference to the human cardiovascular system.

Figure 8 Human cardiovascular and arteriovenous connection network

The human circulatory network is a closed-loop system consisting of cardiac structures, arterial pathways, capillary networks, and venous channels, as shown in Fig. 8. In a bionic electrohydraulic actuator, the fluid transfer network consists of four main components: a pressure supply conduit for the servo valve, a return conduit, a rod and column conduit, and a non-rod conduit. The anatomical layout of the arteriovenous network in biological systems provides valuable insight into optimizing these hydraulic channels. To accurately replicate the morphology of the vascular junctions, a cubic Bessel curve algorithm was used for geometric modeling.

In a biomimetic fluid conduit construction, the rotary distributor annular chamber functions similarly to a heart structure in a biological system. After flowing from the rotary chamber, the hydraulic medium is delivered to the servo valve through a geometrically optimized Bessel curve conduit as previously designed. However, to minimize flow losses within the flow channel, the machined single hydraulic flow channel can be integrated with the fractal cardiovascular model shown in Fig. 9 to transition to a multi-channel design. The hydraulic flow channel of the integrated bionic electrohydraulic actuator is also affected by factors such as flow rate, pressure, number of branches and layout angle. Therefore, it is necessary to further analyze and design the parameters of the fractal flow channel to optimize the performance.

Figure 9 Fractal cardiovascular mode

According to Poiseuille's law, assuming that blood is incompressible, when a fluid with a viscosity coefficient of μ flows in a horizontal tube with a radius of r, if the pressure difference between the two ends of the fluid with a length of L is Δp, the blood flow is: $q(mL/s)$:

$$q=\frac{\pi r^4 \Delta p}{8\mu l} \tag{1}$$

In the process of laminar flow, the liquid is subjected to internal friction of the pipe wall, resulting in a pressure difference Δp, which is related to the radius change. According to Poiseuille's law, the energy consumed by blood to overcome resistance is shown in Equation (2):

$$E_1=q\Delta p=\frac{8\mu q^2 l}{\pi d^4} \tag{2}$$

Providing nutrition requires energy consumption as shown in Equation (3):

$$E_2=br^a l,\ 1\le a\le 2 \tag{3}$$

The calculation formulas of the primary vessel length l and the secondary vessel l_1 are as Equation (4):

$$\begin{cases} l=L-H/tg\theta \\ l_1=L-H/\sin\theta \end{cases} \tag{4}$$

The calculation formula of the total energy E consumed during blood flow is shown in Equation (5):

$$\begin{aligned} E&=E_1+E_2=E(r,r_1,\theta) \\ &=\left(\frac{kq^2}{r^4}+br^\alpha\right)\left(\frac{L-H}{\tan\theta}\right)+\left(\frac{kq_1^4}{r_1^4}+br_1^\alpha\right)\frac{2(L-H)}{\sin\theta} \end{aligned} \tag{5}$$

According to Equation (5), calculate the partial derivative r, r_1 for respectively, and obtain Equation (6):

$$\begin{cases} \dfrac{\partial E}{\partial r}=0 \\ \dfrac{\partial E}{\partial r_1}=0 \end{cases} \tag{6}$$

And further get the relationship between the primary blood vessel and the secondary blood vessel, such as Equation (7):

$$\frac{r}{r_1}=4^{\frac{1}{a+4}} \tag{7}$$

According to the calculation formula 3.5 of the total energy E consumed in the process of blood flow, and then calculate the partial derivative of θ, get the Equation (8):

$$\frac{\partial E}{\partial\theta}=0 \tag{8}$$

The angle relationship can be obtained, as shown in Equation (9):

$$\cos\theta=2\left(\frac{r}{r_1}\right)^{-4}=2^{\frac{a-4}{a+4}} \tag{9}$$

Under the condition of $1\le a\le 2$, the design domain of vessel radius and angle can be finally determined, as shown in Equation (10):

$$\begin{cases} 1.26\le\dfrac{r}{r_1}\le 1.32 \\ 74^\circ\le 2\theta\le 98^\circ \end{cases} \tag{10}$$

According to Equation (10), the optimal ratio of the radii of the main and branch pipes should be designed in the range of 1.26 to 1.32. Notably, the ratio of 1.26 satisfies Murray's law, which is essential for effective fluid dynamics. For the bifurcation the angle between the main and branch ducts should be designed between 74° and 98°, as this range is consistent with the results of thrombosis analysis. In this range, the rate of thrombus formation in the vessel can be effectively reduced. Considering these factors, a 45° angle was finally chosen for the design.

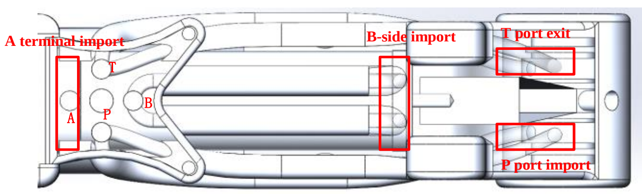

Figure 10 Actuator line port location

During the development of additively manufactured integrated electro-hydraulic actuator cylinders, the runner configuration becomes a key factor affecting the hydraulic transmission performance and system dynamics. Based on the fractal bionic runner structure, we designed a compact rotating fluid distribution mechanism to accommodate the basic hydraulic connections of the actuator: pressure inlet (P), return outlet (T), rod-side port (A), and non-rod-side port (B). The optimized geometric configuration of these hydraulic connections is shown in Fig. 10.

In an additively manufactured electrohydraulic actuator system, the pressure (P) and return (T) ports are connected to a rotary distributor mechanism that facilitates the supply of external hydraulic fluid to the actuator. To accommodate the non-coplanar arrangement of the fluid circuit inlets and outlets, the annular chamber of the rotary distributor utilizes a fractal design. This configuration is connected to the servo valve mounting platform via a hybrid channel that combines Bessel curve segments and linear segments, arranged in a Bessel-Linear-Bessel sequence.

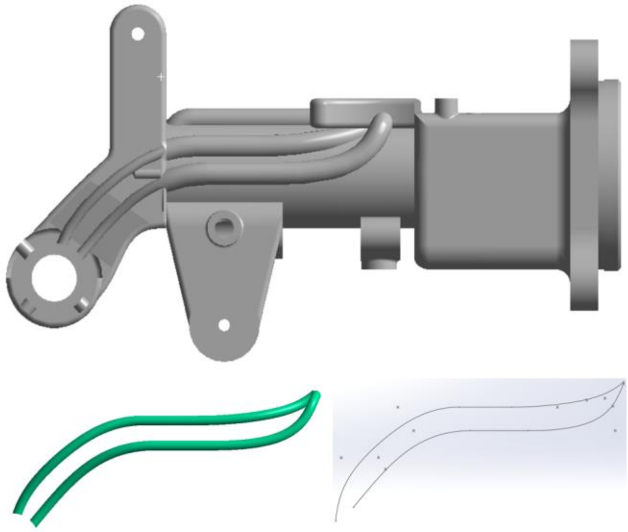

(a) The path of that fluid conduit 1

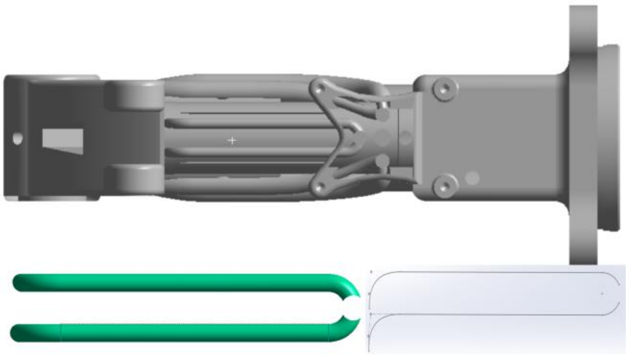

(b) The path of that fluid conduit 2

Figure 11 Actuator fluid conduit line and location

In the additively fabricated electro-hydraulic actuator system, port A establishes hydraulic connectivity with the rod-end chamber, while port B is connected to the non-rod-end chamber, which together enable piston translation and mechanical output generation. The fluid conduit for Port A utilizes a direct linear configuration, while the path for Port B, shown in Fig. 11, utilizes a more complex geometry.

The design conceptualizes the servo cylinder as an annular chamber that is connected to the valve platform by circular, linear and Bezier curve topologies. This optimized flow path geometry enhances fluid dynamics, reduces flow resistance, and improves actuator operating efficiency and dynamic response characteristics.

Additive Manufacturing Integrated Bionic Electro-Hydraulic Actuator Simulation Forming

A comprehensive simulation of the selective laser melting additive manufacturing process of the redesigned hydraulic cylinder barrel assembly was performed by applying Simufact additive software. The simulation parameters are summarized in Table 1.

TABLE I
SIMULATION PARAMETER TABLE

Parameter	Numerical value
Filling spacing	120 μm
Laser power	300W
scanning speed	1300 mm/s
Powder layer thickness	30 μm

During additive manufacturing, parts can be strategically oriented at 45° or 90° relative to the build platform. The 45° placement has several distinct advantages over the 90° orientation. This angular configuration improves stability during the printing process, which greatly reduces the requirement for support structures. As a result, this optimization reduces manufacturing time and material consumption. In addition, the smaller angle between the part surface and the build platform minimizes interlayer gaps, thereby improving the surface quality of the final product.

Fig. 12 shows the simulation results when the holder is placed at 45° for printing. The simulation results show that during the printing process, the maximum stress of the cylinder is 370MPa, the total deformation is 1.31mm, and the maximum displacement is 0.75mm. The material of the cylinder part is 7075 aluminum alloy, and the yield strength of 7075 aluminum alloy is 455Mpa.Combined with the practical experience, the maximum deformation displacement is within the controllable range, which is in line with the requirements.

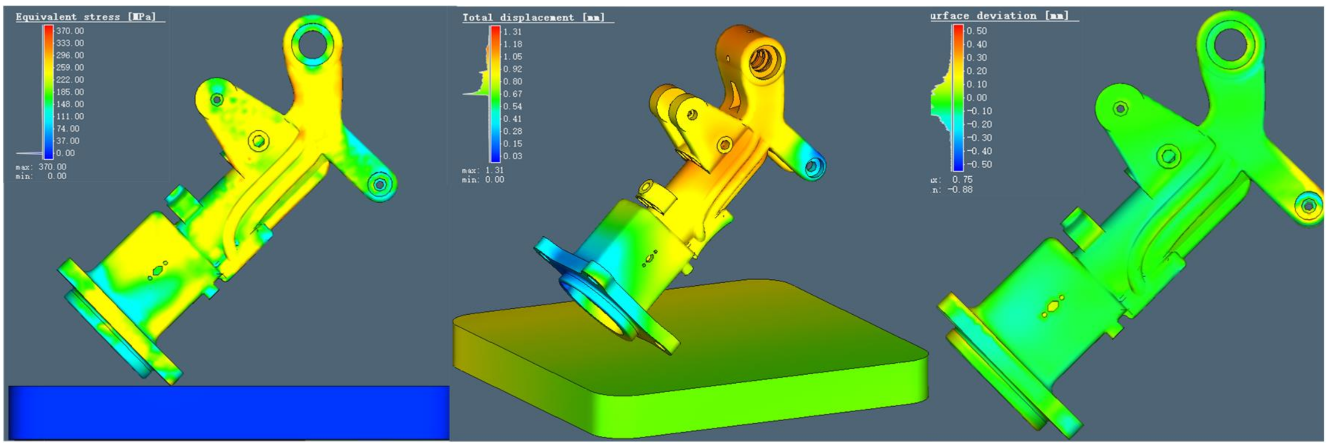

Figure 12 SLM metal additive simulation results when the cylinder is placed in a direction of 45 degrees

C. Runner Optimization Comparison

To verify that the improved integrated bionic electro-hydraulic actuator cylinder meets the required specifications, static analyses were performed under two operating conditions. The results were compared with those of the original integrated electrohydraulic actuator cylinder before structural optimization.

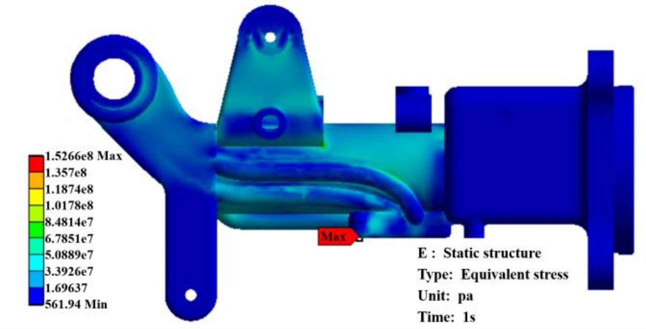

(a) Stress nephogram under working condition 1

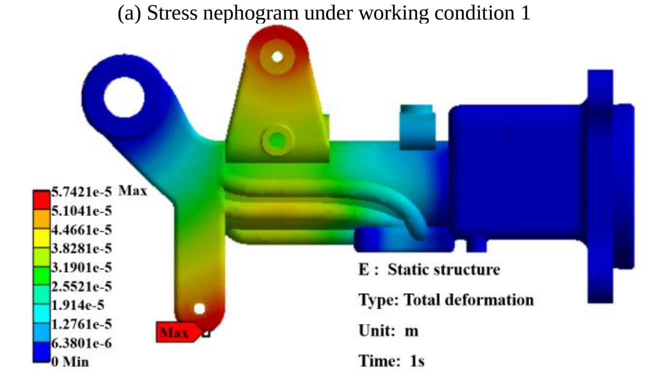

(b) Strain nephogram under working condition 1

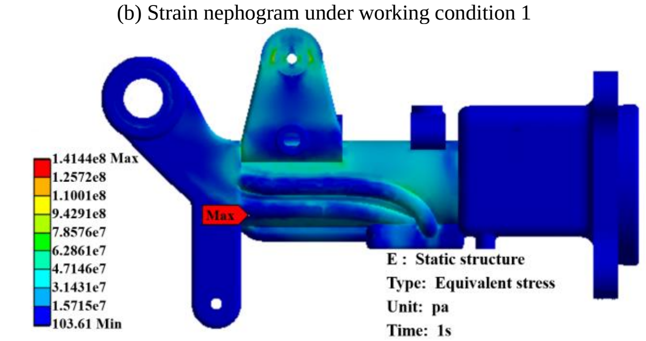

(c) Stress nephogram under working condition 2

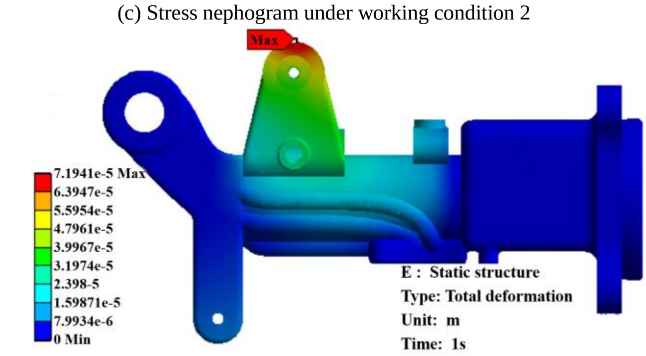

(d) Strain nephogram under working condition 2

Figure 13 Stress-strain cloud diagram of optimized cylinder under working conditions 1 and 2

Fig. 13 shows the stress-strain distribution of the modified cylinder under two different operating conditions. For operating condition 1, the structural analysis shows a maximum von Mises stress of 153 MPa, concentrated at the threaded interface between the hydraulic valve and the cylinder block, and a maximum deformation of 57 μm. It is worth noting that these values imply an increase in stress and deformation of only 13 MPa and 24 μm, respectively, compared to the baseline design. In operating condition 2, the mechanical response exhibits more favorable characteristics, with peak stresses localized in the internal oil passages of 141 MPa and maximum displacements limited to 72 μm. The changes due to optimization are negligible, with only a 6 MPa increase in stress and a 2 micron increase in deformation compared to the original configuration.

Comparative mass and volume before and after optimization are shown in Table 2. The optimization resulted in a mass reduction of about 140 grams, a reduction of about 15%, and a volume reduction of about 50,000 mm, a reduction of about 15%. An effective balance between mass reduction and structural performance maintenance was demonstrated.

TABLE II
COMPARISON OF MASS AND VOLUME OPTIMIZATION OF CYLINDER

Project	Before optimization	After optimization
Mass	916.36 g	776.54 g
Volume	326105.25 mm^3	276349.24 mm^3
Surface area	107730.62 mm^2	104572.96 mm^2

Numerical simulation of the flow channel before and after optimization is performed to analyze and compare the velocity distribution, pressure distribution and flow distribution of the fluid in the flow channel, and then analyze the energy loss of the fluid in different regions. The boundary conditions for numerical simulation are set as inlet velocity and outlet pressure. According to the mechanical design manual, the inlet velocity is 2.5m/s, the outlet pressure is 10 MPa, and the fluid medium is 35# aviation hydraulic oil with a density of 850kg/m2 and a kinematic viscosity of 0.03965 m2/s. The inlet velocity is 2.5m/s and the outlet pressure are 10 MPa.

A comparison of the flow path simulations before and after optimization is shown in Fig. 14. Fig. 14(a) and (b) show that in the pre-optimized flow channel, the fluid is subjected to a large centrifugal force when passing through the elbow section, resulting in the formation of vortices and secondary flow patterns. These flow perturbations result in an uneven pressure distribution throughout the flow channel. In contrast, the optimized design shown in Fig. 14(c) and (d) shows significantly uniform pressure distribution and complete suppression of vortex formation, indicating a substantial improvement in the flow characteristics.

Fig. 15 shows the simulation results comparing the runner performance at point B of the cylinder before and after optimization. As shown in Fig. 15(a) and (b), the pre-improved runner design exhibits significant flow perturbation when the fluid passes through the bend. The sudden change in flow direction leads to a drastic change in the fluid flow line, resulting in a localized velocity surge and the formation of a backflow vortex. In addition, the gradual expansion of the cross-sectional area of the runner downstream of the bend enhances the flow spreading and increases the fluid resistance and friction losses. In contrast, the optimized design shown in Fig. 15(c) and (d) significantly improves the flow pattern. The fluid pressure distribution in the channel is highly uniform and the generation of vortices is eliminated.

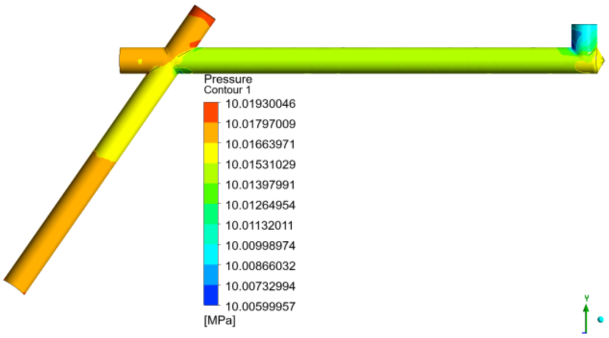

(a) Optimized front runner pressure nephogram

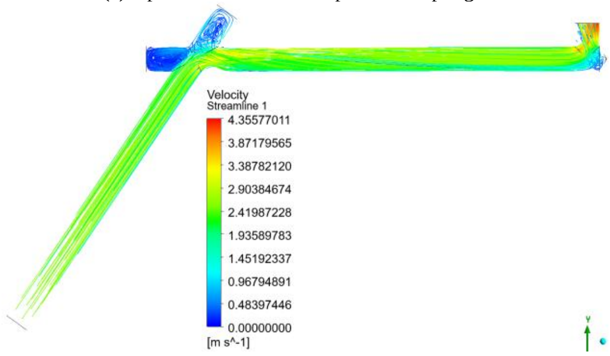

(b) Optimized front runner velocity nephogram

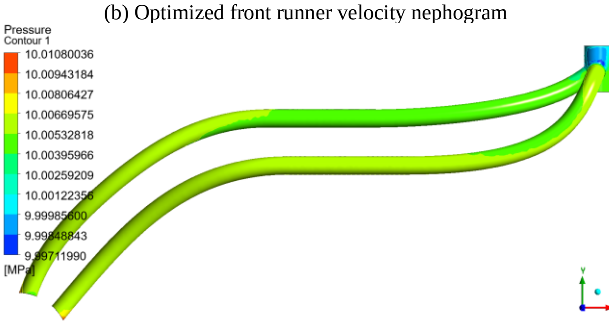

(c) Optimized flow runner pressure nephogram

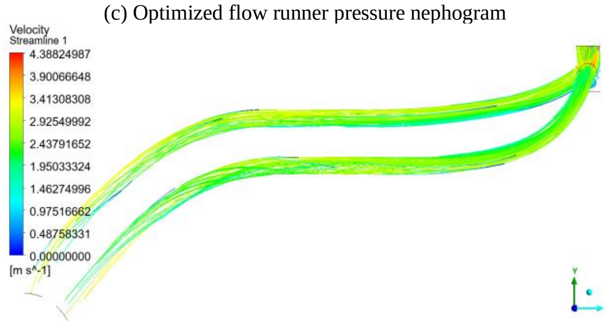

(d) Optimized flow runner velocity nephogram

Figure 14 Simulation comparison diagram of runner before and after

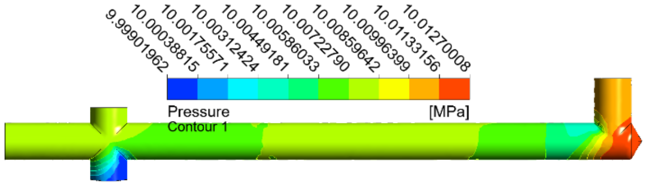

(a) Optimized front runner pressure nephogram

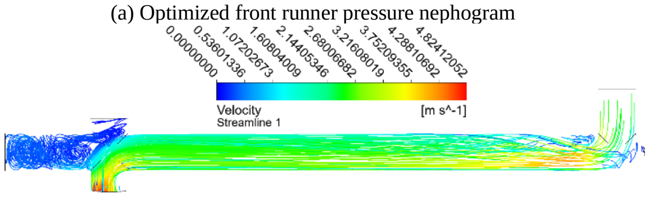

(b) Optimized front runner velocity nephogram

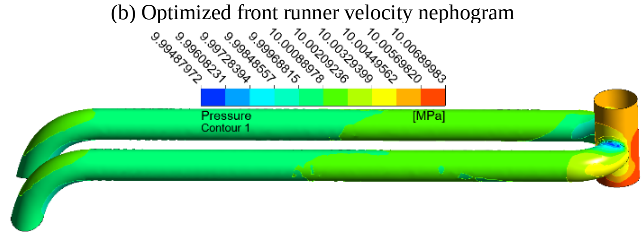

(c) Optimized flow runner pressure nephogram

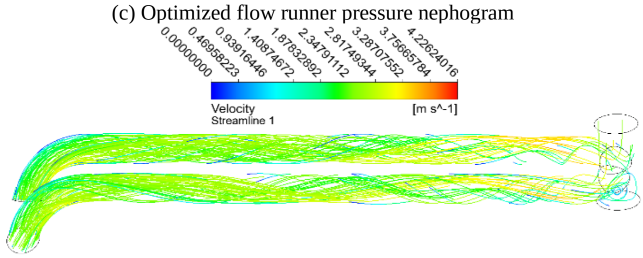

(d) Optimized flow runner velocity nephogram

Figure 15 Simulation Comparison Diagram of Point B runner before and after Optimization

A comprehensive quantitative evaluation of the hydraulic losses of the runners was performed and the evaluation data are shown in Table 3. The pressure distribution of the runners for conventional and additive manufacturing was analyzed and compared. The experimental results show that the additive manufacturing flow channel has more superior performance, and the pressure loss is significantly reduced compared with the conventional machining flow channel under the same conditions of exit velocity and pressure. Specifically, the pressure loss of the conventional system was 0.0188 MPa at PT and 0.0106 MPa at B. The pressure loss of the conventional system is significantly lower than that of the conventional system. By implementing the Bessel curve transition zone in the optimized design, these losses were reduced to 0.0108 MPa (PT) and 0.0048 MPa (B), or 42.55% and 54.71%, respectively. This optimization significantly improves the energy transfer efficiency by more than 40% over conventional manufacturing runners.

TABLE III
COMPARISON OF PRESSURE LOSS OF ADDITIVE MANUFACTURING ACTUATORS

Piping model	Inlet Pressure/Mpa	Outlet pressure/Mpa	Pressure Loss/Mpa	Compared with the linear transition pressure loss reduction percentage/%
Traditional pipeline at PT	10.0188	10	0.0188	/
Optimized pipeline at PT	10.0108	10	0.0108	42.55
Traditional pipeline at B	10.0106	10	0.0106	/
Optimized pipeline at B	10.0048	10	0.0048	54.71
Traditional pipeline at PT	10.0188	10	0.0188	/
Optimized pipeline at PT	10.0108	10	0.0108	42.55
Traditional pipeline at PT	10.0188	10	0.0188	/

IV. CONCLUSION

In this study, based on the existing machined integrated electro-hydraulic actuator, the integrated bionic electro-hydraulic actuator was redesigned by integrating topology optimization, bionic vascular runner design and additive manufacturing technology. And the corresponding static analysis, additive manufacturing simulation analysis and runner simulation analysis were carried out. The results show that the difference of stress and strain under various working conditions before and after optimization is very small, which ensures that the design meets the requirements of practical applications, while the mass and volume of the electro-hydraulic actuator cylinder are reduced by 15%, which meets the requirements of lightweight. Simulation results show that the pressure loss of each runner is reduced by more than 40% after optimization, and the energy transfer efficiency is significantly improved. This paper successfully applies the fusion of topology optimization and additive manufacturing, which provides a new idea for the research of electro-hydraulic actuators for legged robots.

REFERENCES

[1] Barasuol, V., Villarreal-Magaña, O. A., Sangiah, D., Frigerio, M., Baker, M., Morgan, R., ... & Semini, C. (2018). Highly-integrated hydraulic smart actuators and smart manifolds for high-bandwidth force control. Frontiers in Robotics and AI, 5, 51.

[2] Elasswad, M., Tayba, A., Abdellatif, A., Alfayad, S., & Khalil, K. (2018). Development of lightweight hydraulic cylinder for humanoid robots applications. Proceedings of the Institution of Mechanical Engineers, Part C: Journal of Mechanical Engineering Science, 232(18), 3351-3364.

[3] Hansen, M. R., & Andersen, T. O. (2005). System topology optimization. Australian Journal of Mechanical Engineering, 2(2), 133-141.

[4] Hirose, S., & Kato, K. (2000, April). Study on quadruped walking robot in Tokyo Institute of Technology-past, present and future. In Proceedings 2000 ICRA. Millennium Conference. IEEE International Conference on Robotics and Automation. Symposia Proceedings (Cat. No. 00CH37065) (Vol. 1, pp. 414-419). IEEE.

[5] Hyon, S. H., Yoneda, T., & Suewaka, D. (2013, November). Lightweight hydraulic leg to explore agile legged locomotion. In 2013 IEEE/RSJ International Conference on Intelligent Robots and Systems (pp. 4655-4660). IEEE.

[6] Khan, H., Kitano, S., Gao, Y., Caldwell, D. G., & Semini, C. (2015, May). Development of a lightweight on-board hydraulic system for a quadruped robot. In 14th Scandinavian International Conference on Fluid Power-SICFP.

[7] Khan, H., Kitano, S., Frigerio, M., Camurri, M., Barasuol, V., Featherstone, R., ... & Semini, C. (2015, May). Development of the lightweight hydraulic quadruped robot—MiniHyQ. In 2015 IEEE international conference on technologies for practical robot applications (TePRA) (pp. 1-6). IEEE. https://doi.org/10.1109/TePRA.2015.7219671, 2015b.

[8] Kitano, S., Hirose, S., Endo, G., & Fukushima, E. F. (2013, November). Development of lightweight sprawling-type quadruped robot TITAN-XIII and its dynamic walking. In 2013 IEEE/RSJ International Conference on Intelligent Robots and Systems (pp. 6025-6030). IEEE.

[9] Kubo, S., Yaji, K., Yamada, T., Izui, K., & Nishiwaki, S. (2017). A level set-based topology optimization method for optimal manifold designs with flow uniformity in plate-type microchannel reactors. Structural and Multidisciplinary Optimization, 55, 1311-1327.

[10] Li, Y., Li, B., Ruan, J., & Rong, X. (2011, September). Research of mammal bionic quadruped robots: A review. In 2011 IEEE 5th International Conference on Robotics, Automation and Mechatronics (RAM) (pp. 166-171). IEEE.

[11] Liu, G., Zhang, J., & Xu, B. (2019, April). Structure optimization for passages in hydraulic manifolds using metal additive manufacturing technology. In 2019 IEEE 8th International Conference on Fluid Power and Mechatronics (FPM) (pp. 485-492). IEEE.

[12] Zong, H., Zhang, J., Jiang, L., Zhang, K., Shen, J., Lu, Z., ... & Xu, B. (2024). Bionic lightweight design of limb leg units for hydraulic quadruped robots by additive manufacturing and topology optimization. Bio-Design and Manufacturing, 7(1), 1-13.

[13] Meek, S., Kim, J., & Anderson, M. (2008, May). Stability of a trotting quadruped robot with passive, underactuated legs. In 2008 IEEE International Conference on Robotics and Automation (pp. 347-351). IEEE.

[14] Gao J, Xiao M, Zhang Y et al (2020) A comprehensive review of isogeometric topology optimization: methods, applications and prospects. Chin J Mech Eng 33(1):87.

[15] Shi G, Guan C, Quan D et al (2020) An aerospace bracket designed by thermo-elastic topology optimization and manufactured by additive manufacturing. Chin J Aeronaut 33(4):1252–1259.

[16] Yang JK, Gu DD, Lin KJ et al (2022) Laser additive manufacturing of bio-inspired metallic structures. Chin J Mech Eng Addit Manuf Front 1(1):100013.

[17] Huang H, Zhang JH, Xu B et al (2021) Topology optimization design of a lightweight integrated manifold with low pressure loss in a hydraulic quadruped robot actuator. Mech Sci 12(1):249–257.

[18] Mosher, R. (1968). Test and evaluation of a versatile walking truck. In Proceedings of Off-Road Mobility Research Symposium, Washington DC, 1968 (pp. 359-379).

[19] Playter, R., Buehler, M., & Raibert, M. (2006, May). BigDog. In Unmanned Systems Technology VIII (Vol. 6230, pp. 896-901). SPIE.

[20] Semini, C. (2010). HyQ-design and development of a hydraulically actuated quadruped robot. Doctor of Philosophy (Ph. D.), University of Genoa, Italy.